Local buckling resistances of cold-formed high-strength steel SHS and RHS with varying corner radius

Lu Yang[a], Fei Yin[a], Jie Wang[b,*], Azrat Bilal[b], Ari Habeeb Ahmed[b], Manfang Lin[a]

[a] Faculty of Architecture, Civil and Transportation Engineering, Beijing University of Technology, China
[b] Department of Architecture and Civil Engineering, University of Bath, U.K.
[*]Corresponding author. E-mail address: j.wang@bath.ac.uk

Abstract:

This paper reports an experimental and numerical study of the cross-sectional behaviour of cold-formed high-strength steel (HSS) square and rectangular hollow section (SHS and RHS) members. Six stub column tests, six 3-point and three 4-point bending tests have been carried out, followed by the development of accurate finite element (FE) models and a parametric study. Based on the test and FE results, the design rules for slender cross-sections in European, American, Australian and Chinese standards and the GSRM method have been assessed via reliability analyses. A new equation for deriving the cross-sectional slenderness of SHS and RHS considering the influence of corner radius and new area reduction factors for designing slender cold-formed S900 (and above) SHS and RHS have also been proposed.

Keywords: Cold-formed steel structures, Effect of corner radius, High strength steels, Local buckling, Square and rectangular hollow sections (SHS and RHS), Stub column tests, 3-point bending tests, 4-point bending tests.

1. Introduction

High-strength steels (HSS) are defined as steels with nominal yielding strengths greater than

460 MPa (and up to 1100 MPa) and are currently widely available in the market. Their superior strength to weight ratio has motivated their wide application, as can be evidenced by the increasing number of landmark constructions worldwide [1][2]. Meanwhile, the design rules for structural HSS are being developed, which mainly involve the assessments of the applicability of current design rules that were originally designed for ordinary strength steels (e.g. EN 1993-1-1 [3], AISC 360-16 [4], AS 4100 [5] and GB 50017 [6]) on high strength steel members. The European standard, EN 1993-1-12 [7], serves as one of the only few official design provisions that cover the design of HSS up to S700, and the design against stability is largely a simple extension of the design rules in EN 1993-1-1 [3] set out for conventional steel structures.

Focusing on the design of cold-formed HSS square and rectangular hollow sections (SHS and RHS), a review of relevant literatures is given herein. Ma et. al. has carried out a series of experimental and numerical studies on S700 and S900 SHS and RHS stub columns [8][9] and beams under 4-point bending [10][11]. Compared to the 4-point bending test and FE data [11], the plastic and yield slenderness limits set out in EN 1993-1-1 [3], AISC 360-16 [4] and AS 4100 [5] were shown to be conservative, and new slenderness limits were proposed [11]. For the design of slender (Class 4) cross-sections, the Effective Width Method (EWM) [12] and the Direct Strength Method (DSM) [13] were shown to overestimate slightly the axial resistances of S700, S900 and S1100 SHS and RHS [9] while underestimate significantly their moment capacities [11]. To this end, new safety factors were proposed for the design of slender cold-formed HSS SHS and RHS stub columns [9] and a less conservative DSM equation adopting modified parameters was proposed for designing the beams [11]. Feldmann et. al. [14] have also carried out a series of stub column tests on cold-formed S500, S700 and S960 SHS and found that the EWM [12] was slightly unsafe compared to the test data, which was in an agreement with the observations made by Ma et. al. [8][9]. They have also pointed out that how the original plate width is taken in SHS and RHS has a great impact on the result, and hence suggested to use the whole cross-section slenderness, as can be obtained by finite strip method [13][15], for the assessment of design methods for slender SHS and RHS.

The material properties and residual stresses of cold-formed S700 and S900 SHS and RHS members were studied in Ma et. al. [16], where the bending residual stresses were measured as 40% - 60% of the 0.2% proof strength on average. These were significantly larger than the measured membrane residual stresses which reported a maximum value of only 20% of the 0.2% proof strength. The magnitudes of residual stresses were also shown to be higher in the transverse direction than in the longitudinal direction [16]. Somodi & Kovesdi [17] also carried out residual stress measurements on cold-formed SHS and RHS across a larger range of steel grades (S400, S420, S500, S700 and S960), and drew similar conclusions as in Ma et. al. [16] that the longitudinal membrane residual stresses in cold-formed HSS SHS and RHS are negligible. For this reason, only characterisation models for the bending residual stresses were proposed [17]. In the subsequent research on the overall structural performance of these cold-formed sections, as in Ma et al. [9][11] and Somodi & Kovesdi [18], the longitudinal membrane residual stresses were ignored in the numerical models developed.

In summary, the research works reviewed above have investigated the local buckling behaviour of cold-formed HSS SHS and RHS and proposed residual stress models and cross-sectional design rules. However, in these studies, the influence of corner geometry on the resistance of cold-formed HSS tubular sections has not received enough attention. It was found that as the steel grade increases, the inner corner radius required for the cold-forming process also increases, from as low as 0.5t in S500 steels to as high as 3.5t in S900 and S1100 steels [19]. This will render the current assumption for SHS and RHS design in different standards inaccurate: simply taking the flat width as the calculation width as in EN 1993-1-3 [20], AISI S100 [21], AS/NZS 4600 [22] and GB 50017 [6], or assuming the corner region is 0.5t as in EN 1993-1-5 [12] are deemed not accurate. Furthermore, current design methods developed based on SHS and RHS with smaller corner radii may not be accurate for higher strength steel SHS and RHS with significantly larger corner radii.

To this end, the current work aims at investigating the influence of corner radius on the local buckling resistance of cold-formed SHS and RHS and assessing the applicability of current design methods on the test and FE data generated based on a practical range of corner radii. A series of tensile coupon tests, geometric measurements, stub column tests, 3-point and 4-point bending tests are carried out on S700 and S900 SHS specimens, which are then used for validating numerical models and consequently generating parametric results considering a wider range of steel grades and geometric dimensions. Based on the test and FE results, the current design methods for cold-formed structures in EN 1993-1-3 [20], AISI S100 [21], AS/NZS 4600 [22] and GB50017 [6], and the generalized slenderness-based resistance method (GSRM) [23] are assessed. A newly proposed design method, considering the influence of corner radius and developed based on the framework of GSRM [23], has also been proposed and validated against the obtained results.

2. Experimental study

2.1 General information

An experimental program investigating the compressive and bending behaviours of cold-formed HSS SHS sections is described in this section. A series of tensile coupon tests, geometric imperfection measurements, stub column tests and beam tests were carried out in the Structures Laboratory at the University of Bath. The specimens covered two cold-formed steel grades and three SHS cross-sectional sizes, including S700 80×3, S700 100×3, and S900 80×3.5. The SHS specimens were manufactured by cold-rolling process and the S700 and S900 materials have nominal proof stresses of 700 MPa and 900 MPa, respectively. Fig. 1 depicts the geometric shape of the SHS, with B, H, t and r_i denoting the outer width, outer height, wall thickness and inner corner radius of the cross-section, respectively.

2.2 Tensile coupon tests

To obtain the material properties of the investigated cold-formed SHS, a series of tensile coupons were extracted from the specimens and tested according to the procedures set out in EN ISO 6892-1 [24]. For each section, three flat coupons machined from the central regions of 3 faces (F1-F3 in Fig. 1 and Fig. 2(a)) and two corner coupons (C1 and C2 in Fig. 1 and Fig. 2(b)) were prepared, resulting in a total of 15 tensile coupons. A 50 kN Instron testing frame was used to carry out the tensile coupon tests at a strain rate of 0.00007/s before yielding and 0.00024/s afterwards [24].

The stress-strain curves of the tested flat and corner coupons are shown in Fig. 3. The key average material properties are summarised in Table 1, where E is the Young's modulus, $\sigma_{0.2}$ is the 0.2% proof stress considered as the yield stress, $\sigma_{1.0}$ is the 1.0% proof stress, σ_u is the ultimate tensile strength, ε_u is the strain at σ_u, ε_f is the plastic strain at fracture calculated based on the elongation over the standard gauge length of $5.65\sqrt{A_c}$, where A_c is the cross-sectional area of the coupon, and n and m are the Ramberg-Osgood strain hardening parameters [25]. As shown in Fig. 3, all the coupons exhibited rounded stress-strain relationships without a sharply defined yield point and the corner coupons displayed higher strengths and lower ductility than their flat counterparts, as can be attributed to the fact that the cold forming process introduced highly localised plastic strains in the corner regions. It should be noted that some of the corner coupons in this study exhibited very high stiffness, which may be attributed to a small extend of flattening of the curved coupons under the tensile loading. Therefore, a Young's modulus of 210 GPa was adopted as the averaged value for the corner coupons (Table 1). The averaged tested Young's moduli were 223, 192 and 251 GPa for the S700-80×3, S700-100×3 and S900-80×3.5 corner coupons, respectively.

2.3 Geometric imperfection measurements

The local geometric imperfection measurements were performed using a Faro 3D scanner. The geometric profiles were scanned and exported as point clouds, which were then post-processed using MATLAB [26]. The imperfection measurement was only conducted on the six stub column specimens, and the measured values were considered to be representative for the cross-sections investigated, as the local imperfection is defined as the maximum deviation of the central line to the averaged edges of each faces [27]. It was unrealistic to scan the beam specimens due to that, firstly, their very large sizes did not fit the scanning table, and secondly, the failure regions of the beams were localised at where the bending moment was maximised during the test which means that the maximum deviation may not correspond to the actual location where local buckling occurred. The maximum imperfection amplitude among the four faces of each section was taken as the imperfection magnitude w_0, as reported in Table 2 for the six stub columns. The maximum out-of-flatness tolerance for cold-formed steels specified as $w_{EN} = 0.008B$ (B is the width of the plate, see Fig. 1) according to BS EN 10219-2 [28] is also given in Table 2 for each section. As can be seen from Table 2, all the stub column specimens fulfilled the BS EN 10219-2 [28] requirement, and in general a higher imperfection amplitude is associated with a higher plate slenderness $c/(t\varepsilon)$, where $c = B\text{-}2t\text{-}2r_i$ and $\varepsilon = \sqrt{\sigma_{0.2}/235}$, as can be seen for the S700 80×3 and S700 100×3 specimens in Table 2.

2.4 Stub column tests

A total of six stub column tests (2 repeated tests for each cross-section) were carried out. The geometric dimensions of the stub columns are presented in Table 2, where L is the length of the stub column. The nominal column lengths were chosen to be three times the section width to allow the full local buckling deformation to be captured while being short enough to preclude the global buckling failure mode. The stub column tests were performed using a DARTEC 2000 kN hydraulic testing machine, where the specimens were fixed-supported at both ends except that the axial deformation at the loading end was allowed. A displacement control loading method was adopted for all the stub column tests with a speed of 0.5 mm/min. During the test, the average end-shortening δ was measured by two Linear Variable Displacement Transformers (LVDTs) placed at two opposite corners of the specimen, the strain development was monitored by four strain gauges mounted at the mid-height of the specimen and at a distance equal to four times the wall thickness from the external plane of the adjacent face, as illustrated in Fig. 1, and the load was read from the loading jack directly.

All the stub columns failed by a typical local buckling mode, as shown in Fig. 4. The load-end shortening (N-δ) curves for all the stub columns are plotted in Fig. 5. The key test results are reported in Table 2, including the ultimate load N_u, the end shortening δ_u at N_u, the normalised compressive capacity N_u/N_y, where $N_y = A\sigma_{0.2}$, and the nondimensional plate slenderness $\bar{\lambda}_p$ defined according to EN 1993-1-5 [12] accounting for a width of B-2t-2r_i, for each specimen.

2.5 3-point and 4-point bending tests

Six 3-point bending tests and three 4-point bending tests giving a variant of moment gradients were carried out to investigate the effects of cross-sectional slenderness and moment gradient on the moment resistance of cold-formed HSS SHS beams. The measured dimensions of the beams are given in Table 3, where L_0 is the clear span between the supports. The lengths of the beam specimens were designed to give a variant of moment gradient while long enough to preclude shear failure modes.

The test setups for 4-point and 3-point bending tests are depicted in Figs. 6(a) and 6(b), respectively. Steel rollers were used as supports to facilitate a simply-supported boundary condition. Wooden blocks, with dimensions tightly matching those of the inner faces of the sections, were inserted within the SHS beams at the support and loading point locations to prevent web crippling. The deflections of the beams were measured by means of both string pots and LVDTs placed at mid-span for the 3-point bending tests and at mid-span and two loading points for the 4-point bending tests. The end-rotations of the beams were measured by two inclinometers positioned at the support locations. The strain development was monitored by two pairs of strain gauges attached to the top and bottom flanges (as shown in Figs. 6(a) and 6(b), with the face with welds being the web to minimise its influence on the plate buckling behaviour under compression) and located at the mid-span of the 4-point bending specimens and at a distance of 50 mm to the mid-span of the 3-point bending specimens. The 4-point loading was achieved by a spreader beam with the loading points located at the third points of the specimens (Fig. 6(a)), giving a central span of 533.3 mm. All the beam tests were carried out on a 2000 kN hydraulic loading machine under displacement control with a speed of 2 mm/min.

All the 3-point bending and 4-point bending specimens displayed a failure mode of local buckling of the compression flange and the compressive part of the web, as shown in Fig. 7. The normalised mid-span moment-rotation (M-θ) and moment-curvature (M-κ) responses are plotted in Fig. 8(a) and (b) for the 3-point and 4-point bending specimens, respectively. In Fig. 8(a), θ is the mid-span rotation of the beams under 3-point bending determined as the sum of the two end rotations, and θ_{pl} is the elastic component of the rotation corresponding to the plastic moment capacity M_{pl}, calculated as $\theta_{pl} = M_{pl}L_0/(EI)$. In Fig. 8(b), κ is the curvature of the central span of the beams under 4-point bending derived using the vertical displacements at the two loading points and the mid-span, following the procedure adopted in [29], and κ_{pl} is the elastic component of curvature corresponding to M_{pl} and calculated as $\kappa_{pl} = M_{pl}/(EI)$.

The maximum moments M_u achieved in the tests and the corresponding rotations θ_u (or curvatures κ_u) are reported in Table 3. The cross-section slenderness $c/(t\varepsilon)$ and the elastic and plastic moment capacities M_{el} and M_{pl} of each specimen are also given in Table 3 for comparison purposes. As expected, the results follow the general trend that the higher the cross-sectional slenderness, the lower the moment resistance, and M_u of all the specimens exceeded M_{el} whereas only the stockiest section S900 80×3.5 reached M_{pl}. The moment-rotation curves of 3-point bending samples followed a linear relationship up to the peak moment as the failure was localised next to the loading point at the mid-span, whereas the moment-curvature curves of 4-point bending samples all displayed a yielding slope before failure, which can be attributed to the spread of yielding over the central span before failure occurred [30][31]. The effect of moment gradient on the moment capacity of the cold-formed SHS beams is shown insignificant and no clear trend can be observed. This observation is in line with other studies on high strength steel beam tests [30][31], although theoretically specimens under 3-point bending are expected to exhibit slightly higher moment resistances than under 4-point bending [30][31].

3. Numerical study

3.1 Modelling assumptions

Numerical models were developed using the FE package ABAQUS [32] to firstly replicate the experimental results, and subsequently to generate results with wider ranges of geometric dimensions and material grades. To replicate the test results, the measured geometric dimensions (Tables 2 and 3) and material properties were incorporated into the FE models. The stress-strain relationships of the flat and corner coupons (as reported in Fig. 3 and Table 1) were employed to model the flat and corner regions of the FE models, respectively. Previous investigations on cold-formed HSS material properties [8][16] showed that parts of flat portions near the corners were also strengthened due to cold-forming, hence in this study the FE models were assigned extended corner regions, as detailed in the next section. The measured engineering stress-strain curves were translated into the true stress-log plastic strain relationship before being input into the FE models.

The 4-node SHELL element with reduced integration (1 integration point), S4R, was used to mesh the FE models. This element has been widely adopted in modelling the buckling behaviour of thin-walled steel structures under various loading cases [9][11][18][23], and has been shown to be able to replicate the experimental results for steel sections with width-to-thickness ratios ranging from 7 – 96 [9]. The mesh size of the flat area of the flanges was $c/10$ in both the transverse and longitudinal directions, where $c = B\text{-}2t\text{-}2r_i$. The corner region was discretised by 5 elements circumferentially and adopted a mesh size of $c/10$ longitudinally to be consistent with the mesh of the flat area. The boundary conditions in the stub column tests were modelled by coupling the two end cross-sections to two reference points that were fixed except the axial deformation of the one at the loading end. The pinned supports and loading points of beams under 3-point and 4-point bending were modelled by coupling the cross-sections at the support and loading point locations to reference points that were located at the centroid of the corresponding sections. The vertical loads and reaction forces were applied through these reference points. The reference points at the support locations were pinned in the bending plane and fixed out-of-the bending plane. To improve the computational efficiency, only half of the cross-sections was modelled. The modified Riks method [32] was adopted to allow the pre- and post-buckling responses to be traced. Local imperfection defined in the shape of the corresponding first eigenmode was assigned to the stub column and beam models, with a range of amplitudes investigated in the next section.

Residual stresses were not explicitly modelled in this study. Cold-formed structures can be subjected to longitudinal and transverse residual stresses, and the former has a major influence on their structural performance [16]. The longitudinal bending residual stress was implicitly considered through the tensile coupon tests, where the extracted and curved coupons were reintroduced the bending residual stresses by being clamped to a straight profile in the loading machine. Therefore, the tested stress-strain relationships effectively included the bending residual stresses [29]. The membrane residual stresses of cold-formed HSS RHS and SHS were measured in Ma et al. [16] and Somodi & Kovesdi [17], which reported consistently low magnitudes of longitudinal membrane residual stresses, with the maximum value less than 20% of the 0.2% proof stresses. These magnitudes are considered to have a negligible influence on the finite element models [33], hence they were not explicitly modelled in the current study, as similarly treated in previous research on cold-formed structures [11][33][34].

3.2 Model validation

The width of the extended corner region and the amplitude of local imperfection to be adopted in the parametric study were determined through a sensitivity study, which considered a series of combinations of widths of the extended corner region (b_c = 0.5t, t and 2t) and local imperfection amplitudes ($w = c/50$, $c/100$, $c/200$, $c/300$ and w_0). In the model validation, a total of 180 models were created. Table 3 summarises the mean and coefficient of variation (COV) of the ratios of FE-to-test ultimate loads ($N_{u,FE}/N_{u,TEST}$ and $M_{u,FE}/M_{u,TEST}$) achieved in the stub column tests and beam tests for each combination of w and b_c. It shows that that the combination of $w = c/100$ and $b_c = 2t$ gives the best estimation of the test results with mean $N_{u,FE}/N_{u,TEST}$ and $M_{u,FE}/M_{u,TEST}$ ratios of 1.00 and COV of 0.036 and 0.006, and was therefore employed in the parametric study. The extended corner region of $2t$ is in line with previous research on cold-formed HSS sections [9][18][33]. The imperfection amplitude of $c/100$ is of a similar magnitude as the BS EN 10219-2 [28] requirement $0.008B$ (approximately $c/125$) while being slightly on the conservative side. Typical comparisons of the test and FE load-displacement curves of stub columns and moment-rotation (or curvature) curves of beams under 3-point (or 4-point) bending are given in Figs. 9 and 10, respectively. Typical stub column and beam failure modes of the FE models are also compared with the corresponding experimental modes in Figs. 4 and 7, respectively. These numerical and graphical comparisons confirm that the developed FE models can accurately replicate the experimental results and can be used in the subsequent parametric study.

3.3 Parametric study

Following the validation of the FE models, a parametric study was carried out to expand the current data pool and to investigate the effect of corner radius as a new dimensional constraint found for cold-formed HSS sections. The parametric study covered four steel grades (S500, S700, S900 and S1100), twenty cross-section slendernesses ranging from Class 1 to Class 4 according to the Eurocode 3 definition [3], and a practical range of inner corner radii (r_i) as required for cold-forming different steel grades, including $r_i = 0.5t$, t, $1.5t$ and $2t$ for S500, $r_i = 0.5t$, t, $1.5t$, $2t$ and $2.5t$ for S700, and $r_i = t$, $1.5t$, $2t$, $2.5t$ and $3t$ for S900 and S1100, respectively. The input material parameters in the S700 and S900 FE models were defined based on the average coupon test results in Section 2.2 and those in the S500 and S1100 FE models were obtained from previous studies [16][17]. The stress-strain curves for the flat and corner regions for all the steel grades are given in Fig. 11 with the key material properties summarised in Table

1 and Table 6. To eliminate the strength enhancement effect from element interaction, the stub column models employed SHS and the beam models were defined with a depth-to-width ratio of sqrt(k_w/k_f) = 2.44 to give similar plate slenderness $\bar{\lambda}_p$ of the flange and web, where $\bar{\lambda}_p$ is defined in Eqs. (1) and (2), σ_{cr} is the elastic buckling load of the plate, k is the elastic buckling coefficient with $k_w = 23.4$ and $k_f = 4$ for the web (i.e. stiffened plate under bending) and flange (i.e. stiffened plate under compression), respectively, and $c = B\text{-}t$ for the calculation considered herein. The stub column models covered three common widths of 100, 200 and 300 mm and the beam models covered two widths of 100 mm and 200 mm. In total, 1140 stub column models and 1594 beam models were analysed.

$$\bar{\lambda}_p = \sqrt{\sigma_{0.2}/\sigma_{cr}} \quad (1)$$

$$\sigma_{cr} = \frac{kE\pi^2 t^2}{12(1-\nu^2)c^2} \quad (2)$$

3.4 Effect of corner radius

The results from the parametric study show that the corner radius has different influences on the buckling resistances of cold-formed HSS cross-sections in different slenderness ranges. To illustrate this phenomenon, Figs. 12(a) and (b) plot the normalised resistances of S700 SHS 100×100×3 stub columns and S500 RHS 80×195×3 beams under 3-point bending with different cross-sectional slendernesses $\bar{\lambda}_p$, respectively. The horizontal axis in Figs. 12(a) and (b) is r_i/t, and the vertical axis is the obtained compressive capacity, N_u, (or moment capacities, M_u) normalised by the yielding load, N_y, (or elastic moment, M_{el}) of the cross-section, which is further normalised by the case of N_u/N_y (or M_u/M_{el}) at $r_i/t = 1$, to facilitate a straightforward comparison. Increasing the corner radius in SHS and RHS can reduce both the buckling resistance [35] and the cross-sectional area (hence the yield load). The latter is more pronounced than the former in relatively stocky sections (i.e. $\bar{\lambda}_{\mathrm{p}} < 1.0$), thereby leading to significantly increased normalised resistances, as shown in Figs. 12(a) and (b) for both the compressive and bending loading cases. For more slender cross-sections (i.e. $\bar{\lambda}_{\mathrm{p}} > 1.0$), the reduction in the cross-section area by increasing r_{i} is minimal due to the small wall thicknesses whereas the reduction in the buckling resistance is more phenomenal, resulting in reduced normalised resistances as shown in Figs. 12(a) and (b). These need to be considered in the development of design rules for cold-formed HSS sections, as HSS require higher corner radii during cold-forming than normal strength steels.

4 Design methods

In this section, the obtained test and numerical results were used to assess the suitability of the design provisions for cold-form structural steel members in Europe (EN 1993-1-3 [20]), North America (AISI S100 [21]), Australia (AS/NZS 4600 [22]) and China (GB 50017 [6]) and the generalized slenderness-based resistance method (GSRM) [23]. It should be noted that there are other design codes that apply to general steel structures, such as EN 1993-1-1 [3], AISC 360 [4], AS 4100 [5], however, in this paper, only those developed specifically for cold-formed structures are examined. Firstly, the slenderness limits distinguishing compact, semi-compact and slender cross-sections in the current design provisions were examined. Then the design methods in these provisions for calculating the compression and bending resistances of slender (i.e. Class 4, [20]) cross-sections were evaluated, including the effective width method (EWM, as adopted in EN 1993-1-3 [20], AISI S100 [21], AS/NZS 4600 [22] and GB 50017 [6]), the direct strength method, (DSM [13][15], as adopted in AISI S100 [21]) and GSRM [23]. Furthermore, a new design equation for steel grades S900 and above was proposed and examined against the test and FE results.

The suitability of these design rules was assessed based on reliability analyses according to the Annex D of EN 1990 [36]. While detailed reliability analysis procedures may be referred to previous works by the authors [9][11][37], the adopted material and geometric variation parameters are given herein, and the key results as indicated by the partial safety factor γ_{M0} are summarised. The mean to nominal yield strength ratios (i.e. material overstrength) for S500, S700, S900 and S1100 specimens adopted 1.17, 1.15, 1.16 and 0.99, with the coefficient of variation of 0.057, 0.070, 0.083 and 0.072, respectively, as recommended in [14]. The coefficient of variation of the geometric properties V_g was taken as 0.02 [38]. AISI S100 [21] and AS/NZS 4600 [22] adopt the same safety factors for cold-formed steel design and the equivalent partial safety factors γ_{M0} for compression members and flexural members are 1.05 and 1.18, respectively. In EN 1993-1-3 [20] and GB 50017 [6], the compression and bending members are designed employing one safety factor, which is equivalent to γ_{M0} = 1.0 and 1.12, respectively. Therefore, the design rules were assessed against their respective target safety factors.

4.1 Slenderness limits

The cross-sectional classification is a key approach in the design of structural steel sections with plated elements. In general, plated cross-sections are classified into compact, semi-compact and slender sections (as in AISI S100 [21], AS/NZS 4600 [22]), which respectively correspond to the Class 2, 3 and 4 sections according to the Eurocode 3 [3] definition. The compact sections (Class 2) are those able to achieve full plastic moments under bending, the semi-compact sections (Class 3) sections are those that can reach their elastic moments under bending and full cross-section yielding under compression, and the slender (Class 4) sections cannot attain full cross-sectional yielding under compression and elastic moments under bending due to premature local buckling of the plated elements under compression.

The slenderness limits distinguishing these three types of cross-sections for internal (stiffened) elements (as appearing in SHS and RHS) in EN 1993-1-3 [20], AISI S100 [21], AS/NZS 4600 [22], GB 50017 [6] and GSRM [23] are summarised in Table 7, which are expressed in terms of $c/(t\varepsilon)$, where ε is sqrt($\sigma_{0.2}$/235) and c is the plate width under consideration. It should be noted that the plate width c is defined differently in different design codes, as detailed in Table 7. The translation of AISI S100 and AS/NZS 4600 limits (in terms of $\bar{\lambda}_{\mathrm{p}}$) to the $c/(t\varepsilon)$ format adopted the assumption of E = 210000 N/mm^2. The slenderness limits in EN 1993-1-3 [20], A AISI S100 [21], AS/NZS 4600 [22] and GB 50017 [6] were originally developed based on normal strength carbon steels, and those in GSRM [23] were based on hot-finished normal strength steels and high strength steels, therefore their validity for cold-formed high strength steels requires a careful assessment.

While the yield limits (Class 3 limits) for internal elements under bending can be only assessed by the beam results, those for internal elements under compression can be assessed by both the stub column and beam results, as the four flanges of the stub columns and the upper flange of the beams are under uniform compression. Figs. 13(a) and (b) plot the normalised section capacities (i.e. $N_{\mathrm{u}}/N_{\mathrm{y}}$ for stub columns and $M_{\mathrm{u}}/M_{\mathrm{el}}$ for beams) varying against the $c/(t\varepsilon)$ of the flange and web, respectively. The corresponding yield limits in the current design provisions are also given in Figs. 13(a) and (b). It can be seen from Fig. 13(a) that the beam data gives significantly more conservative results than the stub column data, therefore the reliability analyses of the yield limits for internal elements under compression were based on the stub column results only. The unfactored comparisons in Figs. 13(a) and (b) reveal that in general, the GSRM [23] limits are the most accurate yet conservative for both cases. The obtained partial safety factors γ_{M0} are summarised in Tables 8 and compared with the respective target values as given in different design guidance. Table 8 shows that the target partial safety factors of the codified yield limits are generally violated, except for the AISI S100 (AS/NZS 4600) and GSRM ones for internal elements under bending. This suggests that the derived partial safety factors for each steel grade as reported in Table 8 may be adopted for the design of cold-formed HSS SHS and RHS.

The plastic limits (Class 2) can be only assessed by the bending results, as shown in Figs. 14(a) and (b) for internal elements under compression (flange) and bending (web), respectively. The unfactored comparisons in Fig. 14 indicate that the GSRM limits are the most suitable ones among others. The calculated partial factors γ_{M0} for the plastic limits are summarised in Table 9. It can be seen that the GSRM limits require the smallest γ_{M0} (ranging 0.92~1.54) among others and hence are the most suitable. Nevertheless, the derived γ_{M0} values based on the test and FE results are greater than the respective codified γ_{M0} values, apart from the GSRM limit for S500 internal element under bending. Moreover, the derived γ_{M0} value is shown to increase with the steel grade, revealing that the current codified plastic limits for cold-formed HSS SHS and RHS become less suitable as the steel grade gets higher. Overall, it is suggested herein that the GSRM yield and plastic limits should be adopted for the design of cold-formed HSS SHS and RHS in conjunction with the recommended safety factors of 1.0 and those reported in Tables 8 and 9 if higher than 1.0.

4.2 Design of slender (Class 4) cross-sections

Currently, there are mainly three methods in calculating the local buckling resistances of slender (Class 4) cross-sections, including the widely adopted Effective Width Method (EWM) (adopted in Eurocode 3 [20], AISI S100 [21], AS/NZS 4600 [22], GB 50017 [6]), the Direct Strength Method (adopted in AISI S100 [21], AS/NZS 4600 [22]), and the newly proposed generalised slenderness-based resistance method (GSRM) [23]. In this section, the applicability of these methods to cold-formed HSS SHS and RHS considering a practical range of corner radii and steel grades is assessed based on the test and FE data from the current study.

4.2.1 Plate slenderness of SHS and RHS

As detailed in Table 7, the calculation of the plate slenderness (i.e. in terms of $c/(t\varepsilon)$ or $\bar{\lambda}_p$) of SHS and RHS in different design provision adopts different plate width c: EN 1993-1-1 [3], AISI S100 [21] and AS/NZS 4600 [22] use the flat width $c = B\text{-}2t\text{-}2r_i$; GB 50017 [6] adopts $c = B\text{-}2t$; EN 1993-1-5 [12] recommends to adopt $c = B\text{-}3t$ for RHS members; and EN 1993-1-3 [20] used the distance between the centre points of two adjacent corners and this gives $c = B\text{-}2t\text{-}2r_i\text{+}\sqrt{2r_i}$ for RHS. GSRM [23] and DSM [13][15] consider the local buckling of the cross-section as a whole rather than its individual plate element, and suggest to use the elastic critical buckling stress, σ_{cr}, of the whole cross-section to calculate the plate slenderness $\bar{\lambda}_p = \sqrt{\sigma_{0.2}/\sigma_{cr}}$. The software CUFSM [13][15] developed based on constrained and unconstrained finite strip method is commonly used to estimate the elastic critical buckling stress σ_{cr} of thin-walled cross-sections. Additionally, it was found in [33] that the central line width $c = B\text{-}t$ gives the closest estimation of the plate slenderness of SHS as employing the CUFSM. Therefore, different ways of calculating $\bar{\lambda}_{\mathrm{p}}$ are assessed herein using the CUFSM calculated value $\bar{\lambda}_{\mathrm{CUFSM}}$ as the reference. In Fig. 15, the plate slenderness $\bar{\lambda}_{\mathrm{p1}}$, $\bar{\lambda}_{\mathrm{p2}}$, $\bar{\lambda}_{\mathrm{p3}}$ and $\bar{\lambda}_{\mathrm{p4}}$ calculated based on $c = B\text{-}2t\text{-}2r_{\mathrm{i}}+\sqrt{2r_{\mathrm{i}}}$, $B\text{-}2t\text{-}2r_{\mathrm{i}}$, $B\text{-}3t$, and $B\text{-}t$, respectively, for all the cross-sections modelled in the parametric study are compared to their corresponding $\bar{\lambda}_{\mathrm{CUFSM}}$ values. Fig. 15 shows that the central line width $c = B\text{-}t$ gives the closest estimation of $\bar{\lambda}_{\mathrm{CUFSM}}$ with a mean of $\bar{\lambda}_{\mathrm{p4}}/\bar{\lambda}_{\mathrm{CUFSM}} = 0.973$ and COV = 0.015, which is, however, slightly unconservative.

To this end, the current study proposes an alternative hand-calculation method for obtaining accurate and safe $\bar{\lambda}_{\mathrm{p}}$ values for SHS (or RHS) for practical use when CUFSM is not available. Zeinoddini and Schafer [35] reported a study on the effect of large corner radius on the plate buckling strength of cold-formed (or cold-bended) structures, which suggested the adoption of a reduced buckling coefficient, k_{reduced}, as shown in Eq. (3), to calculate the elastic critical buckling stress of plates supported by rounded corners by replacing k in Eq. (2). It should be noted that in [35] k_{reduced} is applied to $c = B\text{-}2t\text{-}2r_{\mathrm{i}}$ (i.e. the flat width of the plate). However, k_{reduced} from Eq. (3) does not apply for those with $r_{\mathrm{i}}/t < 4$, whereas the results in Fig. 12 indicate the need of taking the effect of corner radius into account for cross-sections with smaller r_{i}/t ratios. Therefore, the current study proposes a modification of Eq. (3) to Eq. (4), with the generated k_{reduced} to be used in conjunction with Eq. (5) to calculate the modified plate slenderness, $\bar{\lambda}_{\mathrm{pm}}$. It should be noted that Eq. (4) was proposed based on back calculating the $\bar{\lambda}_{\mathrm{CUFSM}}$ values and assuming a central-line width of $c = B\text{-}t$. The $\bar{\lambda}_{\mathrm{pm}}$ values are also plotted in Fig. 15, closely in line with the $\bar{\lambda}_{\mathrm{CUFSM}}$ values with a mean $\bar{\lambda}_{\mathrm{pm}}/\bar{\lambda}_{\mathrm{CUFSM}} = 0.998$ and a COV =

0.019. It is suggested that the proposed $\bar{\lambda}_{\mathrm{pm}}$ may be adopted for calculating the plate slenderness of thin-walled SHS and RHS when computational tools are not available.

$$k_{\mathrm{reduced}} = (1.08 - 0.02 \cdot \frac{r_{\mathrm{i}}}{t})^2 \cdot k \tag{3}$$

$$k_{\mathrm{reduced}} = (1.01 - 0.02 \cdot \frac{r_{\mathrm{i}}}{t})^2 \cdot k \tag{4}$$

$$\bar{\lambda}_{\mathrm{pm}} = \sqrt{\frac{\sigma_{0.2}}{\sigma_{\mathrm{cr,m}}}} = \frac{B-t}{t}\sqrt{\frac{\sigma_{0.2}12(1-\upsilon^2)}{k_{\mathrm{reduced}}E\pi^2}} \tag{5}$$

4.2.2 Assessment of current design methods for slender cross-sections

The Effective Width Method (EWM) is adopted in EN 1993-1-5 [12], AISI S100 [21], AS/NZS 4600 [22] and GB 50017 [6] for predicting the resistance of plated elements by assuming a part of the plate (i.e. an effective area) achieves full yielding while the remaining area resists zero force. The reduction of the whole area to the effective area, ρ, of a steel plate depends on its boundary condition, stress distribution and slenderness. For internal (stiffened) plates, ρ is expressed as Eq. (6) [12], where ψ is the stress distribution factor, with $\psi = 1$ for elements under uniform compression and $\psi = -1$ for those under bending.

$$\rho = \begin{cases} 1.0 & \text{for } \bar{\lambda}_{\mathrm{p}} \leq 0.5 + \sqrt{0.085 - 0.055\psi} \\ \dfrac{\bar{\lambda}_{\mathrm{p}} - 0.055(3+\psi)}{\lambda_{\mathrm{p}}^2} \leq 1.0 & \text{for } \bar{\lambda}_{\mathrm{p}} > 0.5 + \sqrt{0.085 - 0.055\psi} \end{cases} \tag{6}$$

The Direct Strength Method (DSM) was proposed by Schafer and Peköz [13][15] for estimating the buckling resistance of cold-formed steel members taking into account the combined effects of local and global instabilities simultaneously and has been incorporated in the AISI S100 [21] and AS/NZS 4600 [22]. The design equation of DSM is generalised to apply to both compression and bending loading cases, as given in Eq. (7), where $\lambda_{\mathrm{l}} = \mathrm{sqrt}(N_{\mathrm{y}}/N_{\mathrm{crl}})$ and $\mathrm{sqrt}(M_{\mathrm{el}}/M_{\mathrm{crl}})$ for cross-sections under compression and bending, being N_{crl} and M_{crl} the critical buckling load and moment, respectively, considering both local and global buckling. Since the current study focuses only on the local buckling response, N_{crl} and M_{crl} only account for local plate buckling and λ_{l} is equivalent to $\bar{\lambda}_{\mathrm{p}}$ herein.

$$\frac{N_{\mathrm{u}}}{N_{\mathrm{y}}}\left(\text{or } \frac{M_{\mathrm{u}}}{M_{\mathrm{el}}}\right) = \begin{cases} 1.0 & \text{for } \lambda_{\mathrm{l}} \leq 0.776 \\ \left[1 - 0.15\left(\frac{1}{\lambda_{\mathrm{l}}}\right)^{0.8}\right]\left(\frac{1}{\lambda_{\mathrm{l}}}\right)^{0.8} & \text{for } \lambda_{\mathrm{l}} > 0.776 \end{cases} \tag{7}$$

The generalized slenderness-based resistance method (GSRM) was developed to understand better the behaviour and strength of hollow sections and improve the economy and practicality of design rules dedicated to these types of sections [23]. The GSRM design equation [23] adopts the basic structure of Winter's formula (as used by EWM) with modified factors for slender cross-sections, as shown in Eqs. (8) and (9), where φ_1 and φ_2 indicate the loading conditions with $\varphi_1 = \varphi_2 = 1$ for hollow sections under compression and $\varphi_1 = 1$ and $\varphi_2 = -1$ for those under bending, respectively.

$$\frac{N_{\mathrm{u}}}{N_{\mathrm{y}}}\left(\text{or } \frac{M_{\mathrm{u}}}{M_{\mathrm{el}}}\right) = \frac{1}{\lambda_{\mathrm{L}}}\left(1 - \frac{A}{\lambda_{\mathrm{L}}}\right), \text{for } \lambda_{\mathrm{L}} \geq 0.5 + \sqrt{0.25 - A} \tag{8}$$

$$A = 0.225 + 0.025\psi_2 \frac{1 + \psi_1}{2} \tag{9}$$

The EWM [12], DSM [13][15] and GSRM [23] design curves are compared with the test and FE data in Figs. 16(a) and (b) for cross-sections under compression and bending, respectively. To avoid the inaccuracy sourced from adopting different c values, the assessment was based on $\bar{\lambda}_{\mathrm{CUFSM}}$. It should be noted that the EWM for beam members involves iterations in the calculation process and cannot be expressed by a $\bar{\lambda}_{\mathrm{p}}$-$M_{\mathrm{u}}/M_{\mathrm{el}}$ curve, therefore it is not included in Fig. 16(b). Careful reliability analyses of the EWM, DSM and GSRM based on the test and FE data have also been carried out. Table 10 summarises the required safety factors γ_{M0} for each steel grade and for each design method, where the γ_{M0} values for EWM and GSRM are shown to be smaller than or around 1.0 except those for the S1100 specimens, indicating their suitability for giving safe prediction to the local buckling resistances of cold-formed HSS SHS and RHS, although with some extent of conservativeness. The DSM safety factors are generally larger than 1.0 indicating that higher partial safety factors should be used in conjunction with the method. It should be noted that the higher partial safety factors obtained for the S1100 specimens are mainly attributed to the relatively material overstrength factor used [14]. It is expected that the safety factors for S1100 cross-sections may be re-evaluated once more material data of S1100 steel is available.

4.2.3 Proposed design curve for S900 and higher steel grades

It can be observed in Fig. 16 and Table 10 that the current design method GSRM [23] can accurately predict the local buckling resistances of S500 and S700 cold-formed SHS and RHS under compression and bending, it still underestimates the S900 and S1100 data points. To this end, a new design curve is proposed specifically for the design of S900 and above cold-formed RHS and SHS, as given in Eqs. (10) and (11), which take the format adopted for GSRM [23] (Eqs. (8) and (9)). The constant factors in Eqs. (10) and (11) were derived by least-square fitting considering all the S900 and S1100 datapoints below N_u/N_y or M_u/M_{el} = 1. Consequently, Eqs. (10) and (11) are generalised for both loading cases of uniform compression and bending, with $\varphi_1 = \varphi_2 = 1$ for compression and $\varphi_1 = 1$ and $\varphi_2 = -1$ for bending, respectively. The proposed design curve is also plotted and compared with the test and FE data in Fig. 16. The required safety factors of the proposed design curve for S900 and S1100 specimens are given in Table 10, which are closer but still less than 1.0 for the S900 specimens, indicating their suitability.

In addition, it is recommended to use a safety factor of 1.25 for S1100 specimen based on the existing material data [16].

$$\frac{N_{\mathrm{u}}}{N_{\mathrm{y}}}\left(\text{or } \frac{M_{\mathrm{u}}}{M_{\mathrm{el}}}\right) = \frac{1}{\bar{\lambda}_{\mathrm{p}}}\left(1 - \frac{0.16 + C}{\bar{\lambda}_{\mathrm{p}}}\right), \text{for } \bar{\lambda}_{\mathrm{p}} \geq 0.5 + \sqrt{0.09 - C} \tag{10}$$

$$C = 0.02\psi_2(1 + \psi_1) \tag{11}$$

5 Conclusions

An experimental and numerical study on the local buckling resistances of cold-formed has been carried out. The experimental work included tensile coupon tests, geometric imperfection measurements, 6 stub column tests and 6 three-point bending and 3 four-point bending tests. Finite Element (FE) models have been developed to replicate the experiments, which were then used in subsequent parametric studies considering various steel grades, cross-section dimensions and a practical range of corner radii. Based on the obtained results, the slenderness limits and design rules for slender cross-sections in various design provisions were assessed by means of reliability analyses. The results suggest that among all the design provisions examined, the GSRM [23] is the most suitable method in terms of accuracy and safety, although with some extent of conservativeness for S900 steel and above. To this end, the study proposed a new local buckling design curve in the framework of GSRM [23] for the design of cold-formed HSS SHS and RHS with S900 steel and above. Additionally, a new calculating method for deriving the cross-sectional slenderness of RHS and SHS considering the influence of corner radius has been proposed to be used when computational tools are not available.

Acknowledgements

The authors acknowledge the International Program for Graduate Students at Beijing

University of Technology and National Nature Science Foundation of China (Grant No.51922001), from which the research of this paper was conducted. The authors also would like to acknowledge the world-leading steel manufacturer SSAB (Finland) for the supply of the high strength steel specimens. Mr William Bazeley, the leading technician in the Structures Lab at the University of Bath, is specifically acknowledged for his kind help in setting up the experiments and training support for the students.

References

[1]. Ban H, Shi G. A review of research on high-strength steel structures. P. I. Civil Eng. Str. B. 2018; 171(8): 625-641.

[2]. Lei F, Guangbin X, Yong Y, Junfen Y. and Jian X. The application and research progress of high strength and high performance steel in building structure. IOP Conf. Ser. Mat. Sci. Eng. 2018; 392(2): 022008.

[3]. EN 1993-1-1. Eurocode 3: Design of steel structures - Part 1-1: General rules and rules for buildings. European Committee for Standardization (CEN); 2005.

[4]. ANSI/AISC 360-16. Specification for structural steel buildings. American Institute of Steel Construction; 2016.

[5]. AS 4100. Steel structures. Standard Association of Australia; 1998.

[6]. GB 50017-2017. Code for design of steel structures. Ministry of Housing and Urban-Rural Development of the People's Republic of China (MOHURD); 2003.

[7]. EN 1993-1-12. Eurocode 3: Design of steel structures - Part 1-12: Additional rules for the extension of EN 1993 up to steel grades S 700. European Committee for Standardization (CEN); 2007.

[8]. Ma J, Chan T, Young B. Experimental investigation on stub-column behavior of cold-formed high-strength steel tubular sections. J. Struct. Eng. 2016; 142(5): 04015174.

[9]. Ma J, Chan T, Young B. Design of cold-formed high-strength steel tubular stub columns. J. Struct. Eng. 2018; 144 (6): 04018063.

[10]. Ma J, Chan T, Young B. Experimental investigation of cold-formed high strength steel

tubular beams. Eng. Struct. 2016; 126: 200-209.

[11]. Ma J, Chan T, Young B. Design of cold-formed high strength steel tubular beams. Eng. Struct. 2017; 151: 432-443.

[12]. EN 1993-1-5. Eurocode 3 - Design of steel structures - Part 1-5: Plated structural elements. European Committee for Standardization (CEN); 2006.

[13]. Schafer B. Review: The Direct Strength Method of cold-formed steel member design. J. Constr. Steel Res. 2008; 64(7-8):766-778.

[14]. Feldmann M, Schillo N, Schaffrath S, Virdi K, Björk T, Tuominen N, et al. Rules on high strength steel (RUOSTE): Final report. Publications Office of the European Union, Luxembourg, 2016.

[15]. Schafer B, Peköz T. Direct strength prediction of cold-formed steel members using numerical elastic buckling solutions. In 14th international specialty conference on cold-formed steel structures, 1998.

[16]. Ma J, Chan T, Young B. Material properties and residual stresses of cold-formed high strength steel hollow sections. J. Constr. Steel Res. 2015; 109: 152-165.

[17]. Somodi B, Kovesdi B. Residual stress measurements on cold-formed HSS hollow section columns. J. Constr. Steel Res. 2014; 128:706-720.

[18]. Somodi B, Kovesdi B. Flexural buckling resistance of cold-formed HSS hollow section members. J. Constr. Steel Res. 2017; 128: 179-192.

[19]. STRENX® think thinner, get stronger, SSAB Official website, Link: https://www.ssab.com/products/steel-categories/hollow-section/products

[20]. EN 1993-1-3. Eurocode 3: Design of steel structures - Part 1-3: General rules - Supplementary rules for cold-formed members and sheeting. European Committee for Standardization (CEN); 2005.

[21]. AISI S100. North American specification for the design of cold-formed steel structural Members. American Iron and Steel Institute; 2012.

[22]. AS/NZS 4600. Cold-formed steel structures. Standard Association of Australia; 2018.

[23]. Toffolon A, Meng X, Taras A, Gardner L. The generalized slenderness-based resistance method for the design of SHS and RHS. Steel Constr. 2019; 12(4):327-341.

[24]. BS EN ISO 6892-1. British standard: metallic materials – tensile testing. Part 1: Method

of test at room temperature. European Committee for Standardization (CEN); 2009.

[25]. Gardner L, Yun X. Description of stress-strain curves for cold-formed steels. Constr. Build. Mater. 2018; 189: 527-538.

[26]. Gonzalez R, Woods R, Eddins S. Digital Image Processing Using MATLAB. Publishing House of Electronics Industry, 2009.

[27]. Schafer B, Peköz T. Computational modeling of cold-formed steel: characterizing geometric imperfections and residual stresses. J. Constr. Steel Res. 1998; 47(3): 193-210.

[28]. BS EN 10219-2. Cold formed welded structural hollow sections of non-alloy and fine grain steels. Part 2: Tolerances, dimensions and sectional properties, European Committee for Standardization (CEN); 2006.

[29]. Rasmussen K, Hancock G. Design of cold-formed stainless steel tubular members. II. Beams. J. Struct. Eng. 1993; 119(8): 2368-2386.

[30]. Chan T, Gardner L. Bending strength of hot-rolled elliptical hollow sections. J. Constr. Steel Res. 2008; 64(9): 971-986.

[31]. Gardner L, Nethercot D. Numerical modelling of stainless steel structural components - a consistent approach. J. Struct. Eng. 2004; 130(10):1586-1601.

[32]. ABAQUS 6.14. Hibbitt and Karlsson and Sorensen, Pawtucket, RI.

[33]. Yun X, Gardner L. Numerical modelling and design of hot-rolled and cold-formed steel continuous beams with tubular cross-sections. Thin. Wall. Struct. 2018; 132:574-584.

[34]. Huang Y, Young B. Experimental and numerical investigation of cold-formed lean duplex stainless steel flexural members. Thin-Wall Struct. 2013; 73: 216-228.

[35]. Zeinoddini V, Schafer B. Impact of corner radius on cold-formed steel member strength. 20th International Specialty Conference on Cold-Formed Steel Structures, 2010.

[36]. BS EN 1990. Eurocode: basis of structural design. European Committee for Standardization (CEN); 2002.

[37]. Wang J, Afshan S, Gkantou M, Theofanous M, Baniotopoulos C, Gardner L. Flexural behaviour of hot-finished high strength steel square and rectangular hollow sections. J. Constr. Steel Res. 2016; 121: 97-109.

[38]. Byfield M, Nethercot D. Material and geometric properties of structural steel for use in design. Struct. Eng. 1997; 75(21): 363–367.

Figures

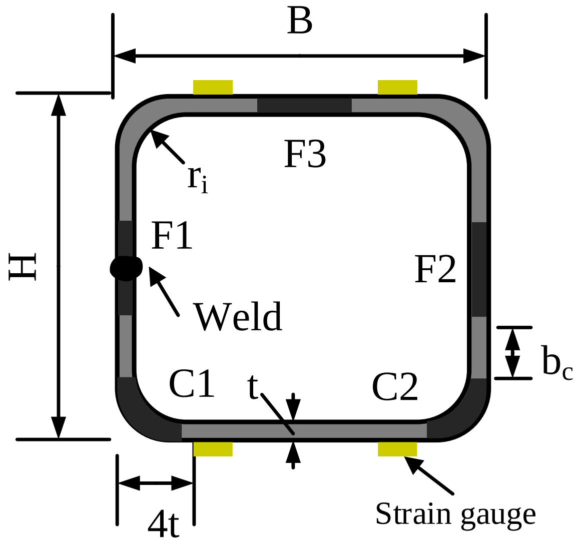

Fig.1 Notations of cross-sectional dimensions and locations of strain gauges

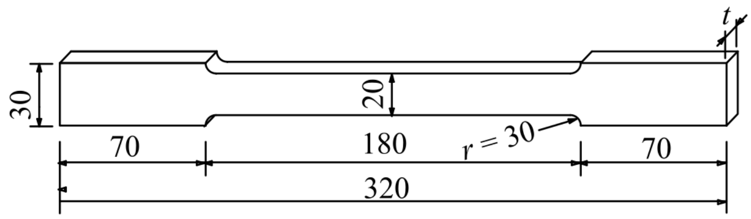

(a) Flat coupon

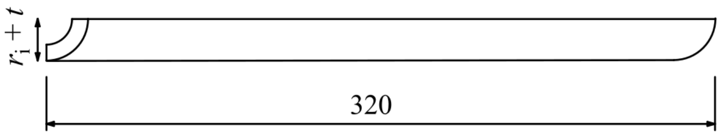

(b) Corner coupon

Fig.2 Dimensions of tensile coupons (unit in mm)

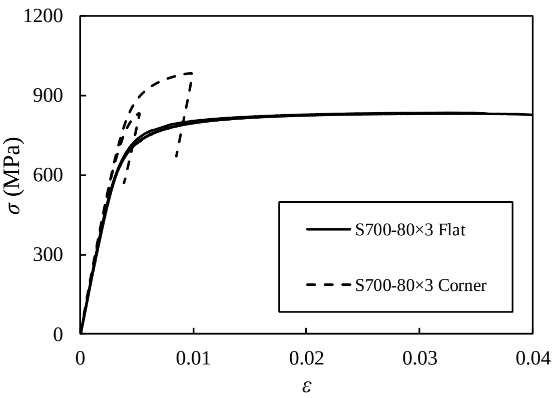

(a) S700 80×3

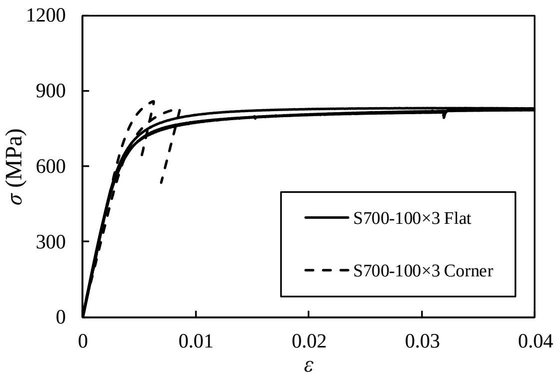

(b) S700 100×3

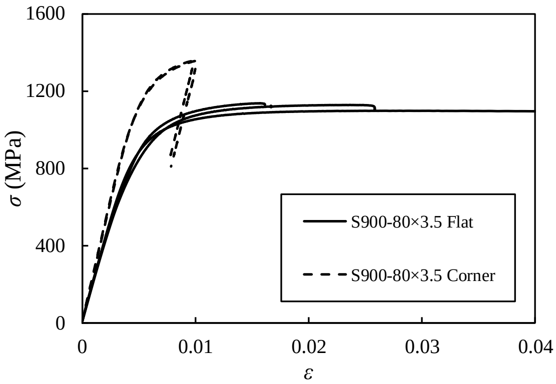

(c) S900 80×3.5

Fig.3 Measured stress-strain curves from tensile coupon tests

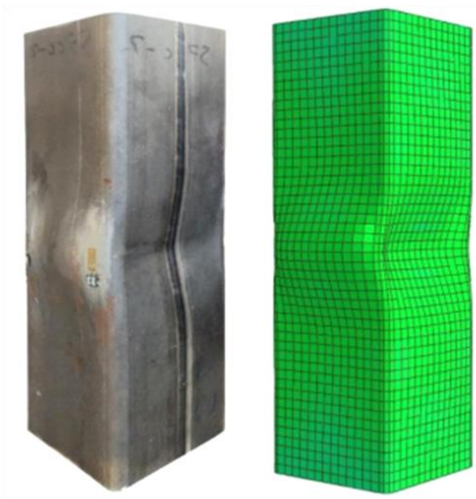

(a) S700 100×3-2

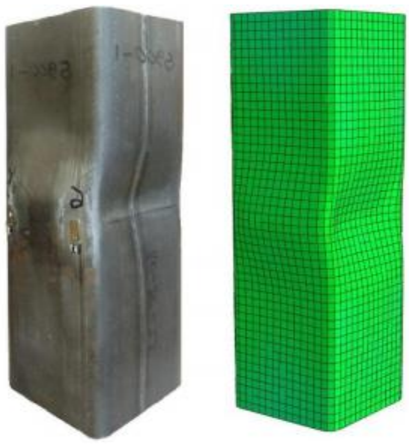

(b) S900 80×3.5-2

Fig. 4 Typical test and FE failure modes of cold-formed HSS SHS stub columns

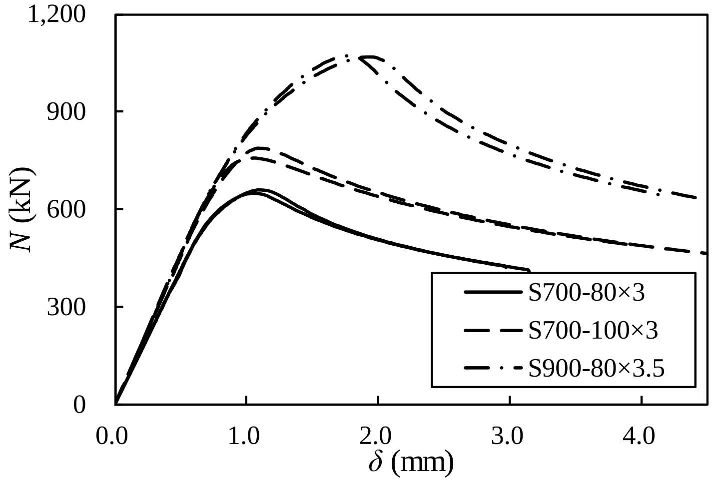

Fig. 5 Load-axial displacement curves from cold-formed HSS SHS stub column tests

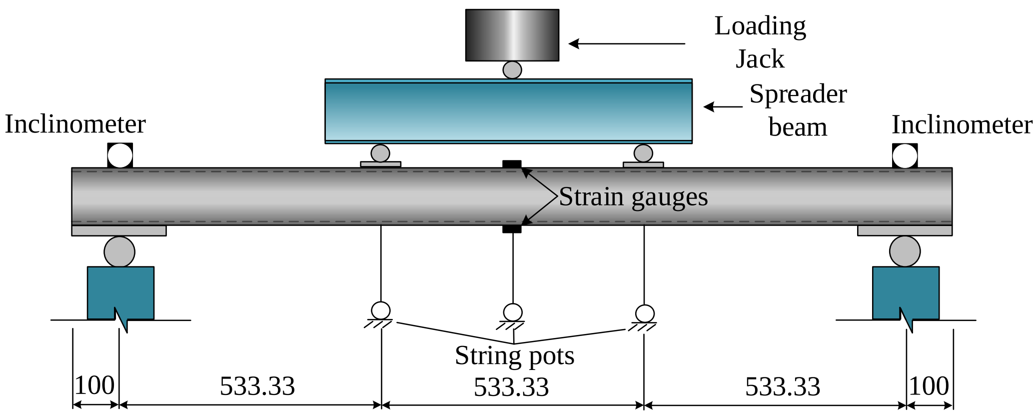

(a) 4-point bending (unit in mm)

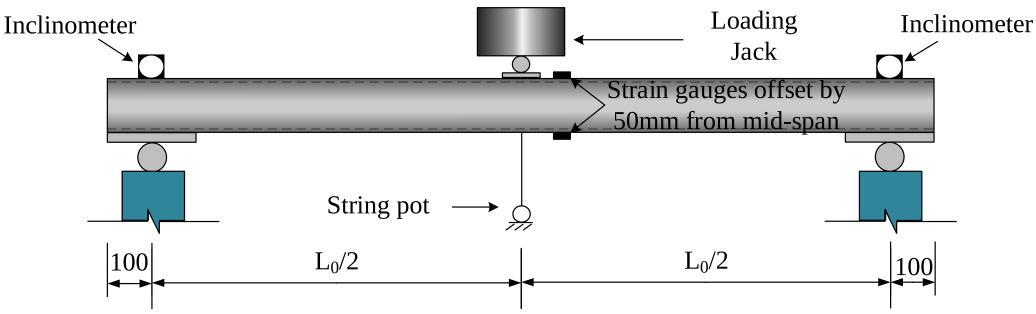

(b) 3-point bending (unit in mm)

Fig. 6 Test setup of bending tests (unit in mm)

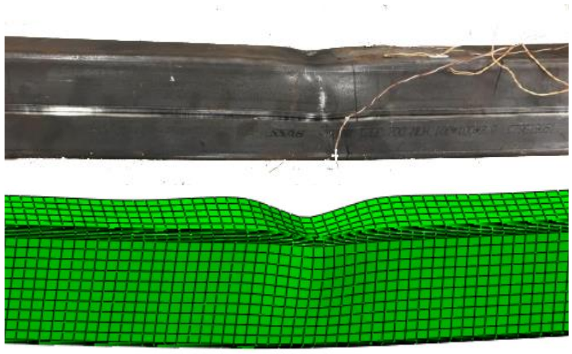

Fig. 7 Typical test and FE failure modes of cold-formed HSS SHS under 3-point bending

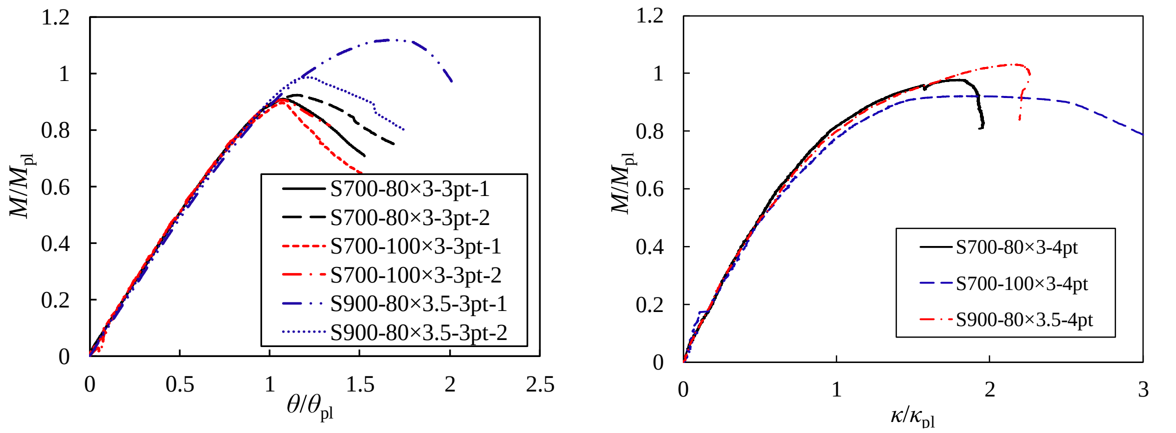

(a) Specimens under 3-point bending (b) Specimens under 4-point bending

Fig. 8 Normalised moment-rotation (or curvature) responses of cold-formed HSS SHS beams under 3-point (or 4-point) bending

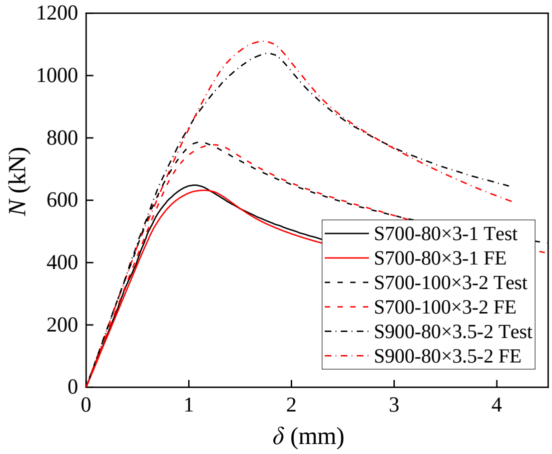

Fig. 9 Comparisons of test and FE load-axial displacement curves of SHS stub columns

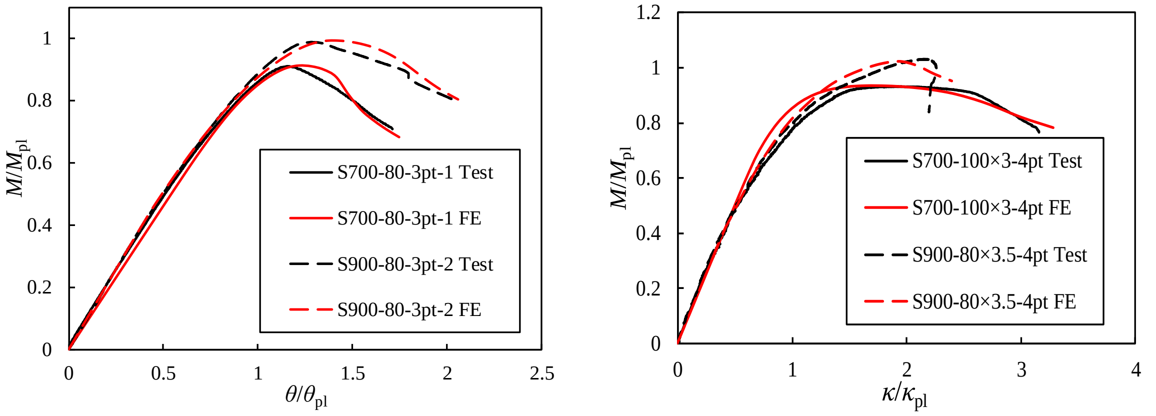

(a) Specimens under 3-point bending (b) Specimens under 4-point bending

Fig. 10 Comparisons of test and FE load vs end-rotation (or curvature) relationships of cold-formed HSS SHS beams under bending

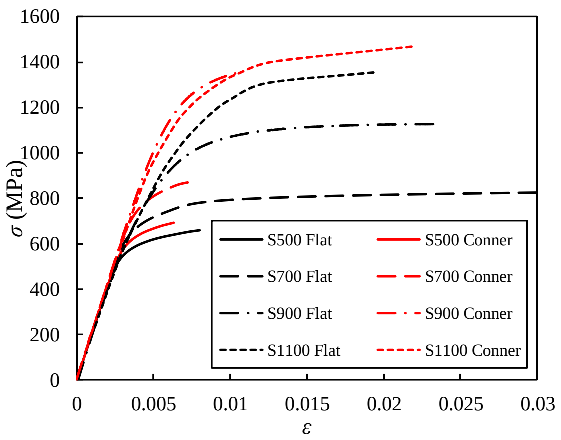

Fig. 11 Material stress-strain relationships employed in the parametric study

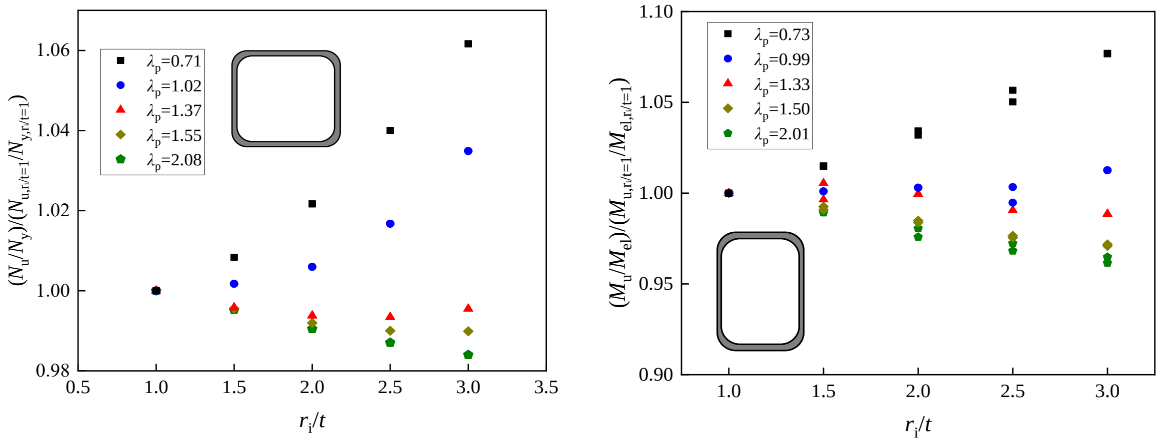

(a) Under compression (S700-100×100) (b) Under bending (S500-80×194-3pt)

Fig. 12 Effect of corner radius on the cross-sectional resistance of cold-formed HSS RHS

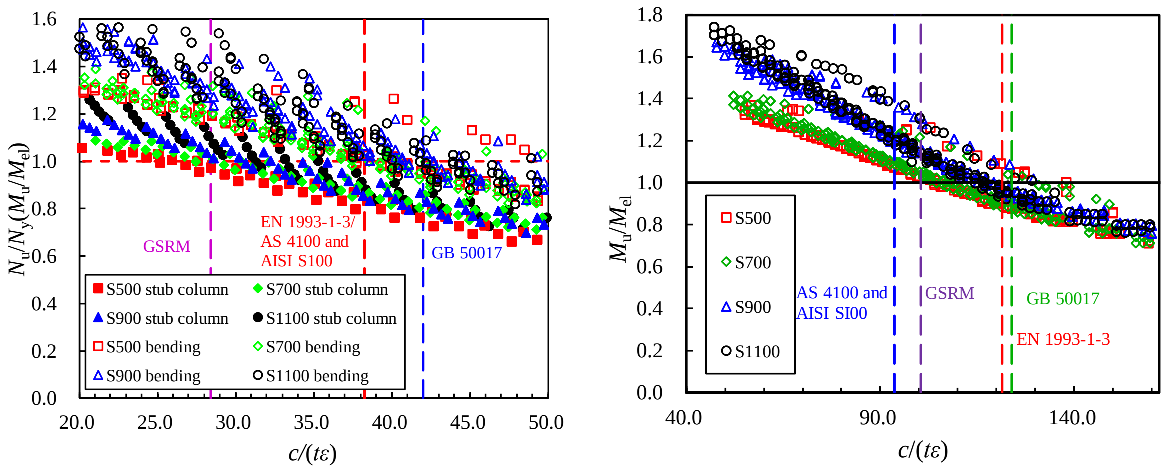

(a) Plates under compression (b) Plates under bending

Fig. 13 Assessment of yield (Class3) slenderness limits in different design provisions

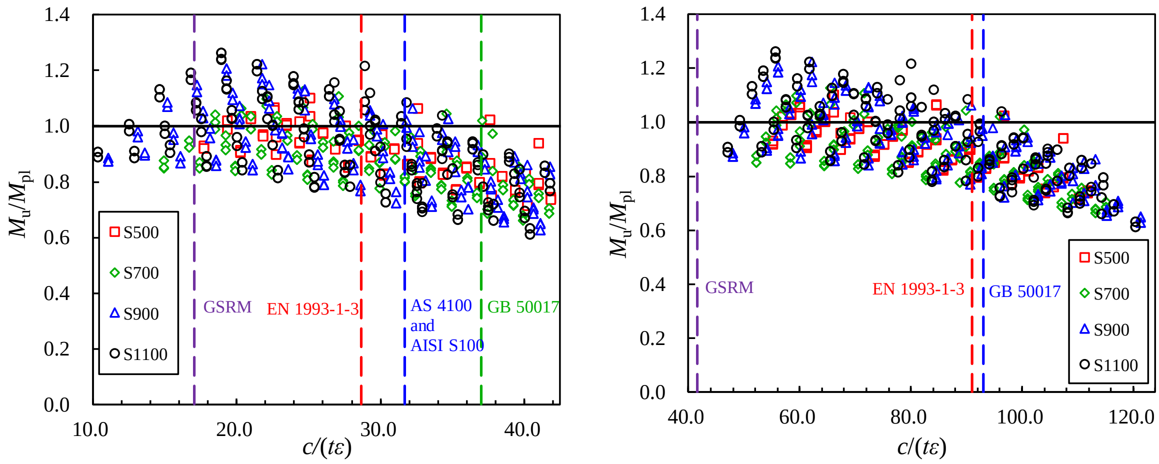

(a) Flange (b) Web

Fig.14 Assessment of plastic (Class 2) slenderness limits in different design provisions

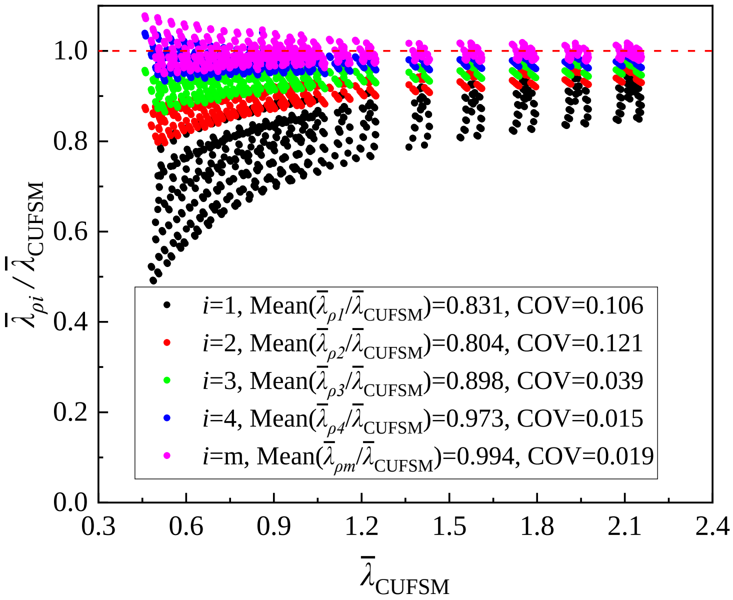

Fig. 15 Comparisons of different definitions of plate slenderness with the CUFSM calculated value

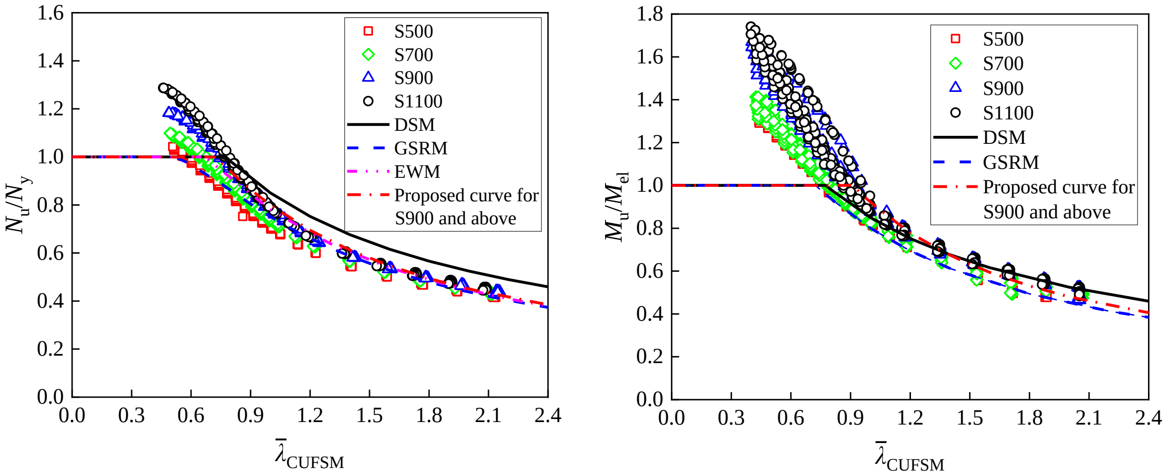

(a) Under compression (b) Under bending

Fig. 16 Assessment of EWM [12], DSM [13][15] and GSRM [23] for the design of cold-formed HSS SHS and RHS

Tables

Table 1 Average material properties obtained from tensile coupon tests

Cross-sections	Coupon	E (MPa)	$\sigma_{0.2}$ (MPa)	$\sigma_{1.0}$ (MPa)	σ_u (MPa)	ε_u (%)	ε_f (%)	m	n
S700-80×3	Flat	208800	755	828	842	2.9	12.6	10.8	4.0
	Corner	210000	926	894	985	1.0	12.2	12.2	4.1
S700-100×3	Flat	204300	731	800	827	4.0	8.5	8.5	3.9
	Corner	210000	860	805	860	0.6	13.5	13.5	4.3
S900-80×3.5	Flat	205900	986	1112	1120	2.3	6.1	6.1	3.9
	Corner	210000	1324	1323	1355	1.0	9.6	22	3.2

Table 2 Measured geometric dimensions and test results of stub columns

Specimens	L (mm)	B (mm)	H (mm)	t (mm)	r_i (mm)	$\bar{\lambda}_p$	w_0 (mm)	N_u (kN)	δ_u (mm)	N_u/N_y
S700-80×3-1	238.5	80.52	80.52	3.02	3.60	0.71	0.594	648.6	1.05	0.93
S700-80×3-2	239.0	80.47	80.48	2.99	3.60	0.72	0.598	657.8	1.10	0.95
S700-100×3-1	299.5	99.96	100.61	3.25	2.80	0.86	0.567	757.9	1.05	0.84
S700-100×3-2	300.0	99.98	100.69	3.25	2.80	0.86	0.532	786.7	1.08	0.87
S900-80×3.5-1	240.0	80.69	80.81	3.52	6.00	0.66	0.315	1070.0	1.93	1.01
S900-80×3.5-2	240.0	80.62	80.75	3.55	6.00	0.66	0.338	1071.1	1.78	1.00

Table 3 Measured geometric dimensions and test results of beam specimens

Specimens	L_0 (mm)	B (mm)	H (mm)	t (mm)	r_i (mm)	$c/(t\varepsilon)$	M_u (kNm)	θ_u (rad) or κ_u	M_u/M_{el}	M_u/M_{pl}
S700-80×3-3pt-1	1600	80.30	80.49	3.08	3.60	39.4	18.25	0.06	1.05	0.91
S700-80×3-3pt-2	1000	80.48	80.457	3.11	3.60	39.1	18.75	0.05	1.07	0.95
S700-100×3-3pt-1	1600	100.46	100.23	3.36	2.80	46.2	30.08	0.05	1.04	0.90
S700-100×3-3pt-2	1000	100.53	100.21	3.28	2.80	47.4	29.77	0.03	1.05	0.91
S900-80×3.5-3pt-1	1600	80.50	80.76	3.69	6.00	34.9	32.86	0.12	1.23	1.08
S900-80×3.5-3pt-2	1000	80.56	80.62	3.56	6.00	36.3	28.97	0.04	1.12	0.99
S700-80×3-4pt	1600	80.46	80.54	3.20	3.60	37.8	20.36	1.91	1.13	0.98
S700-100×3-4pt	1600	100.50	100.12	3.43	2.80	45.1	31.50	1.52	1.07	0.92
S900-80×3.5-4pt	1600	80.47	80.64	3.57	6.00	36.1	30.32	3.08	1.17	1.03

Table 4 Comparison of stub column and beam test results with FE results employing varying widths of extended corner region and amplitudes of local imperfection

Specimens	$b_c = 0.5t$				$b_c = t$				$b_c = 2t$			
	$c/50$	$c/100$	$c/200$	w_0	$c/50$	$c/100$	$c/200$	w_0	$c/50$	$c/100$	$c/200$	w_0
Mean-Stub	0.92	0.98	1.03	1.01	0.92	0.98	1.03	1.01	0.94	1.00	1.05	1.03
COV-Stub	0.034	0.031	0.029	0.044	0.033	0.032	0.031	0.046	0.037	0.036	0.034	0.050
Mean-Beam	0.95	0.97	1.01	0.98	0.96	0.98	1.02	0.99	0.98	1.00	1.04	1.02
COV-Beam	0.015	0.009	0.015	0.013	0.012	0.008	0.005	0.008	0.009	0.006	0.008	0.008

Table 5 Comparisons of test and FE results of stub column and beam specimens.

Specimens		$N_{u,FE}/N_{u,TEST}$ or $M_{u,FE}/M_{u,TEST}$	$\delta_{u,FE}/\delta_{u,TEST}$, $\theta_{u,FE}/\theta_{u,TEST}$ or $\kappa_{u,FE}/\kappa_{u,TEST}$
Stub columns	S700-80×3-1	0.97	1.06
	S700-80×3-2	0.95	1.04
	S700-100×3-1	1.03	1.12
	S700-100×3-2	0.99	1.07
	S900-80×3.5-1	1.02	0.91
	S900-80×3.5-2	1.04	0.98
Beams	S700-80×3-3pt-1	1.00	1.00
	S700-80×3-3pt-2	0.98	0.99
	S700-100×3-3pt-1	1.02	1.50
	S700-100×3-3pt-2	1.01	1.10
	S900-80×3.5-3pt-1	1.01	1.03
	S900-80×3.5-3pt-2	1.00	0.91
	S700-80×3-4pt	0.97	0.99
	S700-100×3-4pt	1.00	0.88
	S900-80×3.5-4pt	0.99	0.91

Table 6 The material parameters in parametric studies

Steel grade	Location	E (MPa)	$\sigma_{0.2}$ (MPa)	σ_u (MPa)	ε_u	Reference
S500	Flat	210000	619.0	659.0	0.0072	[18]
	Corner	210000	672.0	691.0	0.0062	
S1100	Flat	205000	1073.0	1356.0	0.0203	[16]
	Corner	206000	1245.0	1470.0	0.0221	

Table 7 Slenderness limits for cold-formed SHS and RHS beams in current design provisions

Design guidance	Definition of plate width, c	Class 2 flange	Class 2 web	Class 3 flange	Class 3 web
EN 1993-1-3 [20]	$c = B\text{-}2t\text{-}2r_i+\sqrt{2}r_i$	28.68	91.01	38.24	121.35
AISI S100 [21]	$c = B\text{-}2t\text{-}2r_i$	32.4	N/A	38.24	93.64
GB 50017 [6]	$c = B\text{-}2t$	37	93	42	124
GSRM [23]	$c = B\text{-}2t\text{-}2r_i$	17.04	41.65	28.4	100.52

Table 8 Partial safety factors γ_{M0} for the yield (Class 3) limits of cold-formed HSS SHS and RHS

Design guidance	Under compression					Under in-plane bending				
	Target	S500	S700	S900	S1100	Target	S500	S700	S900	S1100
EN 1993-1-3 [20]	1.00	1.28	1.29	1.31	1.43	1.00	1.16	1.19	1.19	1.18
AISI S100 [21]	1.18	1.28	1.29	1.31	1.43	1.05	0.97	0.99	0.99	0.96
GB 50017 [6]	1.12	1.37	1.38	1.45	1.58	1.12	1.17	1.22	1.22	1.21
GSRM [23]	1.00	1.09	1.09	1.04	1.14	1.00	1.00	1.04	1.03	1.01

Table 9 Partial safety factors γ_{M0} for the plastic (Class 2) limits of cold-formed HSS SHS and RHS

Design guidance	Target	Under compression				Under in-plane bending			
		S500	S700	S900	S1100	S500	S700	S900	S1100
EN 1993-1-3 [20]	1.00	1.25	1.39	1.39	1.72	1.16	1.46	1.45	1.69
AISI S100 [21]	1.05	1.30	1.45	1.44	1.79	N/A	N/A	N/A	N/A
GB 50017 [6]	1.12	1.38	1.52	1.52	1.89	1.18	1.47	1.46	1.76
GSRM [23]	1.00	1.10	1.24	1.23	1.53	0.92	1.19	1.18	1.44

Table 10 Partial safety factors γ_{M0} for the design of cold-formed HSS SHS and RHS slender (Class 4) sections

Methods	Cross-sections under compression				Cross-sections under bending			
	S500	S700	S900	S1100	S500	S700	S900	S1100
EWM [20]	0.98	0.96	0.89	1.15	0.99	0.97	1.00	1.29
DSM [13][15]	1.06	1.06	1.01	1.34	1.05	1.05	1.04	1.30
GSRM [23]	0.91	0.91	0.84	1.17	0.95	0.95	0.93	1.15
Proposed	-	-	0.91	1.23	-	-	1.00	1.24